Journal of Applied Physics ARTICLE pubs.aip.org/aip/jap

Search for promising structures and superconductivity in high-pressure Sr through first-principles calculations

Cite as: J. Appl. Phys. **136**, 205901 (2024); doi: 10.1063/5.0230807
Submitted: 26 July 2024 · Accepted: 10 November 2024 ·
Published Online: 25 November 2024

Masaaki Geshi,[1,a)] Hiroki Funashima,[2] and Gayan Prasad Hettiarachchi[1]

AFFILIATIONS

[1]R^3 Institute for Newly-Emerging Science Design, Osaka University, 1-2 Machikaneyama, Toyonaka, Osaka 560-0043, Japan
[2]Department of Comprehensive Engineering, Kindai University Technical College, 7-1 Kasugaoka, Nabari, Mie 518-0459, Japan

[a)]**Author to whom correspondence should be addressed:** geshi.masaaki.insd@osaka-u.ac.jp

ABSTRACT

In the high-pressure phases of Sr, the Sr-V phase is considered an incommensurate host–guest structure. However, just as a low-temperature phase Ba-VI exists in the pressure region of the Ba-IV phase of high-pressure Ba, Sr also has a Sr-VI phase on the low-temperature region of the Sr-V phase according to experiments. We investigated the pressure range from 40 to 2400 GPa using first-principles calculations and found a group of promising candidate structures for the Sr-VI phase. At higher pressures, the lowest-enthalpy structure became hexagonal close-packed (hcp) around 160 GPa and is consistent with experiments for the Sr-VII phase, and the hcp structure transformed to a double hcp (dhcp) structure around 1000 GPa, and then, the dhcp structure changed to a face-centered cubic structure around 2200 GPa. The superconducting state remained intact through these structural phase transitions, although with a decreasing T_c with increasing pressure.

I. INTRODUCTION

Pressure-induced structural phase transitions of Sr have been investigated for more than 60 years, and five phases have been reported experimentally. At ambient pressure, Sr takes a face-centered cubic (fcc) structure (Sr-I). With increasing pressure, the fcc structure transforms to a body-centered cubic (bcc) structure at 3.5 GPa (Sr-II),[1,2] and the bcc structure transforms to the β-tin structure ($I4_1/amd$) at 24 GPa (Sr-III).[3] Next, the β-tin structure transforms to a monoclinic structure with the space group *Ia* and 12 atoms per unit cell at 38 GPa (Sr-IV),[4] and the *Ia* structure then transforms to an incommensurate phase with a host–guest (HG) structure at 46 GPa (Sr-V) and is stable up to 57 GPa. The HG structure then transforms to another accompanying phase at 57 GPa and persists up to at least 75 GPa.[5]

Several computational studies on compressed Sr have been conducted,[6–9] and there remains several discrepancies between the experimental and computational results. One computational work showed that the β-tin structure is not the lowest enthalpy structure compared to the bcc or *Ia* structures in the pressure range of 26–38 GPa suggested by experiments for the β-tin phase.[6] Based on the enthalpy, the sequence of the phase transitions of Sr with increasing pressure was suggested to be fcc, bcc, and Sr-IV. Another study showed that a hexagonal close-packed (hcp) structure takes lower enthalpy than the β-tin, *Ia*, and HG structures.[7] In this work, Srepusharawoot *et al.* used the Sr-V supercell containing 110 atoms with 14 guest and 10 host unit cells with $I4/mcm$ symmetry. They used an incommensurate ratio (γ) of 1.4 in the *c* axis compared with 1.4041 from an experiment.[10]

Kim *et al.* performed a structure search to find the stable structures of Sr up to 50 GPa with simulation cells containing 2, 3, 4, 8, 9, 10, and 12 atoms.[8] They found an orthorhombic structure with space group *Cmcm* symmetry above 25 GPa bringing into question the stability of the HG structure suggested by McMahon *et al.*[5] They also calculated the superconducting transition temperatures T_c up to around 55 GPa assuming the *Cmcm* and bcc structures. Since the difference between the *Cmcm* and hcp structures is small, it is acceptable to consider the hcp structure as suggested by Srepusharawoot *et al.*,[7] however in either case, the suggested structures are not consistent with the experiments.

Tsuppayakorn-aek *et al.* reported that the discrepancy between the experimental and computational results for the β-tin structure can be explained using the screened exchange local density approximation (sX-LDA).[9] However, this is the only case that could be explained by this functional. Hence, it is not sufficient for a final conclusion. Furthermore, the results of the enthalpy were shown for only the hcp, bcc, and β-tin structures, and the effects of considering sX-LDA were not discussed for the other structures of interest for compressed Sr.

Katzke and Tolédano investigated the phase transition mechanisms of alkaline-earth metals theoretically in the framework of an extension of the Landau approach to reconstructive phase transitions.[10] They interpreted all the high-pressure phases as resulting from the full or partial realization of the Burgers and Bain deformation mechanisms. It was further suggested that the high-pressure HG structures of Sr and also Ba reflect the competition between these mechanisms.

Desgreniers *et al.* showed that in the high-pressure phases of Ba, the incommensurate and self-hosting Ba-IV phase is a high-temperature phase realized at room temperature, while there is a much simpler highly symmetric structure at comparable pressure values at low-temperatures, the Ba-VI phase.[11] Their calculations predicted Ba-VI to be dynamically stable at high pressures and to be superconductive. Moreover, Jackson *et al.* reported that T_c of the Ba-VI phase was higher than that of the Ba-IV phase.[12] These results go on to show the potential of cryogenic compression in revealing rich phase diagrams under high pressures.

In light of these findings around the incommensurate HG phase of Ba, and the discrepancies between experiments and theoretical calculations of high-pressure phases of Sr, especially around the experimentally observed highest-pressure HG Sr-V phase, there is a possibility of a highly symmetric structure on the low-temperature and high-pressure region of the incommensurate Sr-V phase. Thus far, to the best of our knowledge, no investigations have been carried out on Sr in the high-pressure region above 100 GPa using first-principles calculations. Very recently, Ito *et al.* reported two new high-pressure phases at low temperatures (Sr-VI and Sr-VII) of compressed Sr after the Sr-V phase and observed the highest T_c of 13 K at 165 GPa experimentally.[13] Although they have not been able to identify the structure of the Sr-VI phase, they have identified the Sr-VII phase as having an hcp structure.

In trying to investigate the low temperature phases of compressed Sr after the Sr-V phase, we performed a structure search based on an original method developed by us[14] in the high-pressure region from around 40–2400 GPa. In addition, we further investigated the phonon profiles and T_c associated with these structures. In particular, the pressure dependence of T_c of the Sr-VI phase is important in determining the actual structure. In this work, we determined a group of plausible structures for the Sr-VI phase and their pressure dependence of T_c, which will be useful for comparison with detailed experimental results when elucidating the actual structure. We also confirmed the Sr-VII phase as having an hcp structure. Herein, we report and discuss these results.

II. COMPUTATIONAL DETAILS

We performed the first-principles electronic structure calculations based on density functional theory (DFT) to determine the crystal and electronic structures of compressed Sr. We used Quantum-Espresso package[15] to perform the total energy calculations, structural relaxations, and phonon calculations with the Perdew–Burke–Ernzerhof (PBE)-type generalized gradient approximation (GGA)[16] as an exchange-correlation functional and ultrasoft pseudopotentials (USPP).[17] The valence electron configuration of Sr is considered to be ten electrons consisting of $4s^2 4p^6 5s^2$. The cutoff radius of the local potential was set to 1.9 a.u., the cutoff energy of the wave function E_{cut} was 80 Ry, and the cutoff energy for the charge density was set twelve times E_{cut}. The Brillouin zone for each structure was sampled using Monkhorst–Pack k-point meshes of $24 \times 24 \times 24$ for four-atom systems, $12 \times 12 \times 12$ for 12 atom systems, $8 \times 8 \times 8$ for 16 atom systems, $4 \times 4 \times 4$ for 32 atom systems, and $2 \times 2 \times 2$ for 64 atom systems. In determining these values, test calculations were performed to ensure that the total-energy precision was sufficient to estimate the differences in the energy and enthalpy between the relaxed structures. The errors were found to be up to 3 meV/atom, and in many cases, smaller. Occasionally, $E_{cut} = 120$ Ry was used for validation purposes in some cases; however, there were no essential differences between the obtained results. Ensuring the computational precision with the aforementioned parameters, we performed an extensive structure search using an original method developed by us.[14,18]

Initial structures from the space group index 75 ($P4$) to 230 ($Ia\bar{3}d$) were generated for a unit cell consisting of four atoms. These cover the tetragonal, trigonal, hexagonal, and cubic structures as the initial structures. The subsequent structural relaxations were performed assuming only the Bravais lattice. In addition, we performed a structure search in a random manner at the given pressure values. We did not perform structural relaxation for all the randomly generated initial structures. Instead, we picked a set of low enthalpy structures obtained from a self-consistent field (SCF) calculation and performed a full optimization on those chosen ones

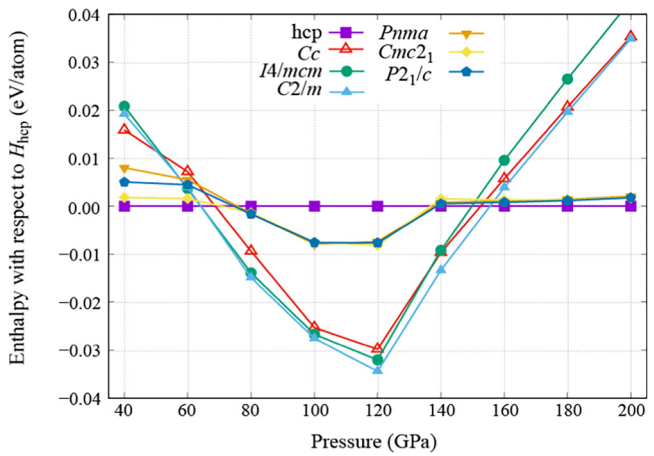

FIG. 1. The calculated enthalpy H of plausible structures pertaining to compressed Sr with respect to the enthalpy of the hcp structure as a function of pressure from 40 to 200 GPa. The solid lines are guides to the eye.

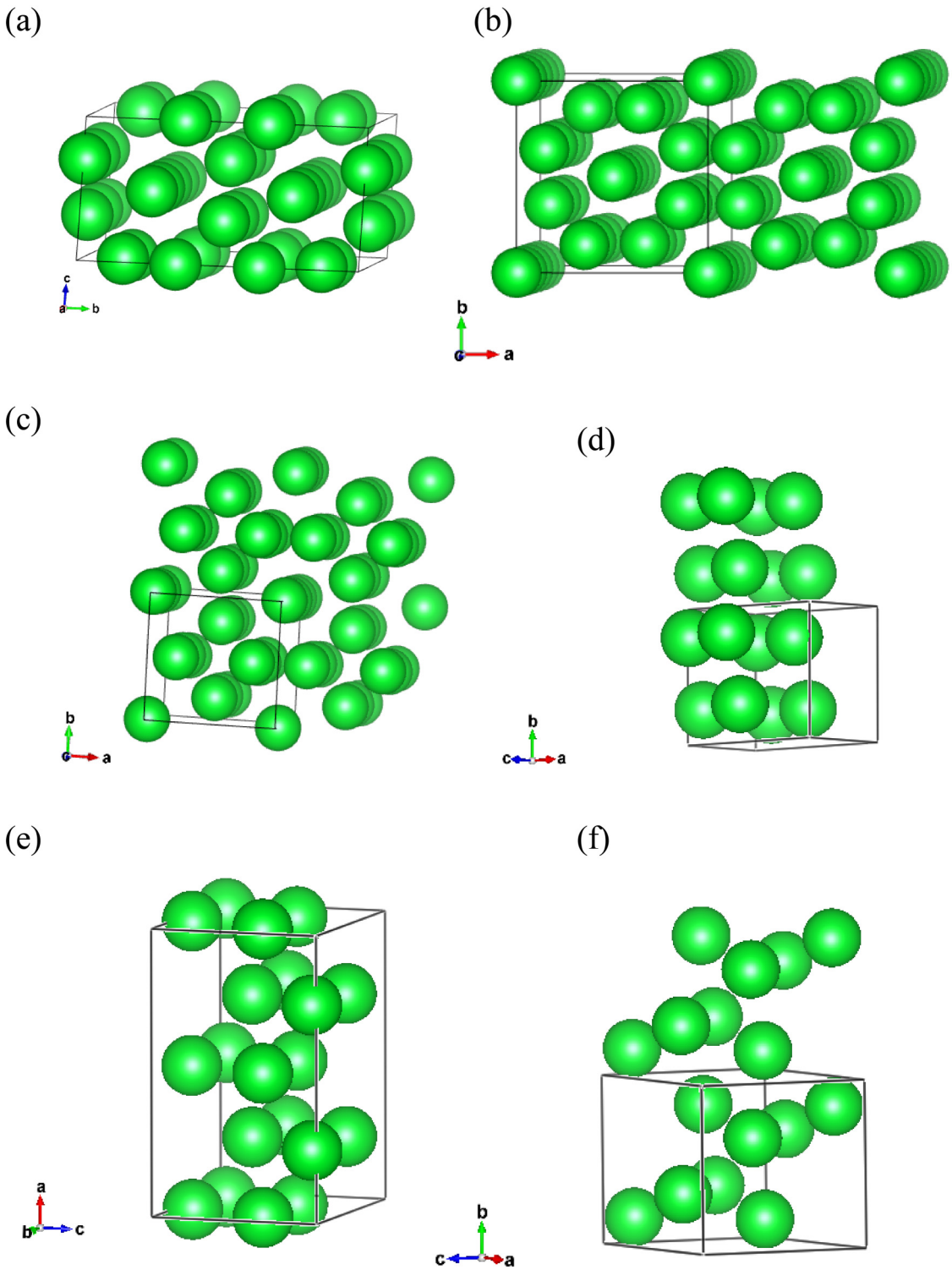

FIG. 2. The atomic structure of (a) *C*2/*m*, (b) *I*4/*mcm*, (c) *Cc*, (d) *Pnma*, (e) *Cmc*2_1, and (f) *P*2_1/*c* structures at 100 GPa. The lattice parameters and atomic positions at 100 GPa are listed in Tables SI–SVII in the supplementary material.

only. We generated 800 initial structures and selected 20 low-enthalpy structures for further investigations.

For phonon calculations, E_{cut} was set to 80 Ry for the fcc, hcp, and double hcp (dhcp) structures, and k-point meshes of $24\times24\times24$, $24\times24\times18$, and $24\times24\times8$ were used for the fcc, hcp, and dhcp structures, respectively. In addition, q-point meshes of $8\times8\times8$, $6\times6\times4$, and $6\times6\times2$ were used for the fcc, hcp, and dhcp structures, respectively.

In calculating T_c, SCF calculation for electron–phonon calculations used a dense grid of k-points. SCF calculation using a grid of k-points was used aiming for good self-consistency, and the phonon calculations were performed for each structure. We used $48\times48\times32$ meshes for the dense grid of k-points and $12\times12\times8$ meshes for SCF and phonon calculations and $6\times6\times4$ q-point meshes for the hcp structure, $24\times24\times24$ meshes for the dense grid of k-points and $6\times6\times6$ meshes for SCF and phonon calculations and $4\times4\times4$ q-point meshes for a $I4/mcm$ structure, $16\times16\times32$ meshes for the dense grid of k-points and $4\times4\times8$ meshes for SCF and phonon calculations and $2\times2\times4$ q-point meshes for a $C2/m$ structure, $32\times32\times48$ meshes for the dense grid of k-points and $8\times8\times12$ meshes for SCF and phonon calculations and $4\times4\times6$ q-point meshes for a $Pnma$ structure, $16\times16\times16$ meshes for the dense grid of k-points and $4\times4\times4$ meshes for SCF and phonon calculations and $4\times4\times4$ q-point meshes for a $Cmc2_1$ structure, and $32\times32\times32$ meshes for the dense grid of k-points and $8\times8\times8$ meshes for SCF and phonon calculations and $4\times4\times4$ q-point meshes for a $P2_1/c$ structure. 40 Ry cutoff energy for the wave function and 480 Ry cutoff for charge density were used for the $C2/m$ and $I4/mcm$ structures, 80 Ry cutoff energy for the wave function and 960 Ry cutoff for charge density were used for the $Pnma$, $Cmc2_1$, and $P2_1/c$ structures, and 120 Ry cutoff energy for the wave function and 1440 Ry cutoff for charge density were used for the hcp structure. T_c was calculated according to the Allen and Dyne formula,[19]

$$T_c = \frac{\omega_{\log}}{1.2}\exp\left[\frac{-1.04(1+\lambda)}{\lambda(1-0.62\mu^*)-\mu^*}\right], \quad (1)$$

where $\omega_{\log} = \exp\left[\frac{2}{\lambda}\int\frac{d\omega}{\omega}\alpha^2F(\omega)\log\omega\right]$, λ is the electron–phonon coupling constant, ω is the phonon frequency, and μ^* is an empirical parameter that describes the Coulomb screening. In this work, we set μ^*=0.13. The broadening method was used to calculate λ and ω. The broadening width σ was set to 0.03, except for $C2/m$, which was set to 0.06 as a numerical safety measure, although the T_c value itself carries a difference in the range of ±0.4 K at 0.03. Regarding the cutoff energy of 40 Ry used for the $C2/m$ and $I4/mcm$ structures, we calculated T_c using 60 Ry for the $C2/m$ structure at 100 GPa and confirmed that there was only a difference of 0.24 K from the result obtained with 40 Ry. Therefore, we believe that there is no essential difference.

III. RESULTS AND DISCUSSION

Figure 1 shows the calculated enthalpies of plausible structures hcp, Cc, $I4/mcm$, $C2/m$, $Pnma$, $Cmc2_1$, and $P2_1/c$ for compressed Sr with respect to the enthalpy of the hcp structure as a function of pressure from 40 to 200 GPa. In obtaining these results, a structure search was performed (except for Cc) covering the space groups mentioned earlier with cells containing four atoms. It is noted that below 60 GPa and above 140 GPa, the structures labeled "$Pnma$," "$Cmc2_1$," and "$P2_1/c$" reduced to the hcp structure as a result of a structural relaxation. The enthalpies labelled "hcp," "$I4/mcm$," and "$C2/m$" remain the same even after a structural relaxation.

Below 60 GPa, the lowest enthalpy structure was the hcp one. To confirm the difference between the $Cmcm$ and hcp structures around which some controversies exist, a structural relaxation was performed using the $Cmcm$ structure as the starting structure, which resulted in the hcp structure. It is reasonable to suggest that the stable structure is obtained from first-principles calculations in the pressure region of Sr-IV is the $Cmcm$ structure or its special case, the hcp structure. We conjecture that Sr-IV has the hcp structure. This is reasonable considering the results of previous works,[6–8] and the fact that the cutoff energy of 80 Ry used in our calculations is larger than that of 36.75 Ry (500 eV) used in previous works.

Sr-V is an incommensurate phase and should be explored using cells containing more atoms. Hence, the structure searches were performed using cells containing 12, 16, and 32 atoms, using a random search at 40 and 100 GPa. The $C2/m$ structure was found as the lowest enthalpy structure through the random structure-search based method and the $Pnma$ structure as the second lowest one using cells containing 32 atoms at 100 GPa. The $I4/mcm$ structure was found as the lowest enthalpy structure and the $P2_1/c$, $Pnma$, and $Cmc2_1$ structures were found as the second, third, and fourth lowest enthalpy ones using cells containing 16 atoms at 100 GPa. The $Pnma$ structure was found as the lowest enthalpy structure and the hcp one as the second lowest enthalpy structure using cells containing 12 atoms at 100 GPa. However, the $C2/m$ and $I4/mcm$ structures could not be found using smaller cells. Other than these structures, the Cc structure was also obtained by optimizing the $Fdd2$ structure containing 16 atoms per unit cell shown by Whaley-Baldwin *et al.* as the approximate structure of the HG structure.[20] These seven structures including hcp are the

TABLE I. The atomic positions of the $Pnma$ structure at 100 GPa. The lattice parameters are a = 4.9537, b = 4.0503, and c = 2.9485 Å. The atomic volume is 59.1592 Å^3.

	Wyckoff letter	x	y	z	Wyckoff position
Sr1	4c	0.3334	0.2500	0.0713	(x, 1/4, z)

TABLE II. The atomic positions of the $Cmc2_1$ structure at 100 GPa. The lattice parameters are a = 8.2006, b = 5.8491, and c = 4.9306 Å. The atomic volume is 236.4995 Å^3.

	Wyckoff letter	X	Y	z	Wyckoff position
Sr1	4a	0.000 00	0.662 10	0.107 35	(0, y, z)
Sr2	8b	0.752 19	0.085 46	0.438 42	(x, y, z)
Sr3	4a	0.000 00	0.166 96	0.105 56	(0, y, z)

TABLE III. The atomic positions of the $P2_1/c$ structure at 100 GPa. The lattice parameters are $a = 5.0094$, $b = 4.9516$, and $c = 5.0094$ Å. The atomic volume is 118.7173 Å^3.

	Wyckoff letter	x	y	z	Wyckoff position
Sr1	4*e*	0.837 99	0.834 01	0.090 18	(x, y, z)
Sr2	4*e*	0.662 23	0.333 07	−0.085 56	(x, y, z)

candidate structures for consideration for the Sr-V and Sr-VI phases in this pressure region.

From about 60 to 160 GPa, the *C*2/*m*, *I*4/*mcm*, and *Cc* structures are obtained as one group of lowest-enthalpy structures as plausible candidates for the Sr-V phase. The crystal structures of *C*2/*m*, *I*4/*mcm*, and *Cc* prepared using VESTA[21] are shown in Figs. 2(a)–2(c). Even though the enthalpy is low, the *Cc* structure is dynamically unstable based on the phonon calculations within the harmonic approximation. The *I*4/*mcm* structure is also dynamically unstable, only with the exception at 100 GPa. The *I*4/*mcm* structure found here has the same space group as the structure shown in Ref. 5, which might correspond to the case where the value of the incommensurate ratio of the HG structure may be approximated by 16 atoms. The *C*2/*m* structure is dynamically stable in the entirety of the plotted pressure range and is the most promising candidate for the Sr-V phase as will be discussed later together with the accompanying T_c values and their conformity with the experimental results. The atomic positions of the *C*2/*m* structure at

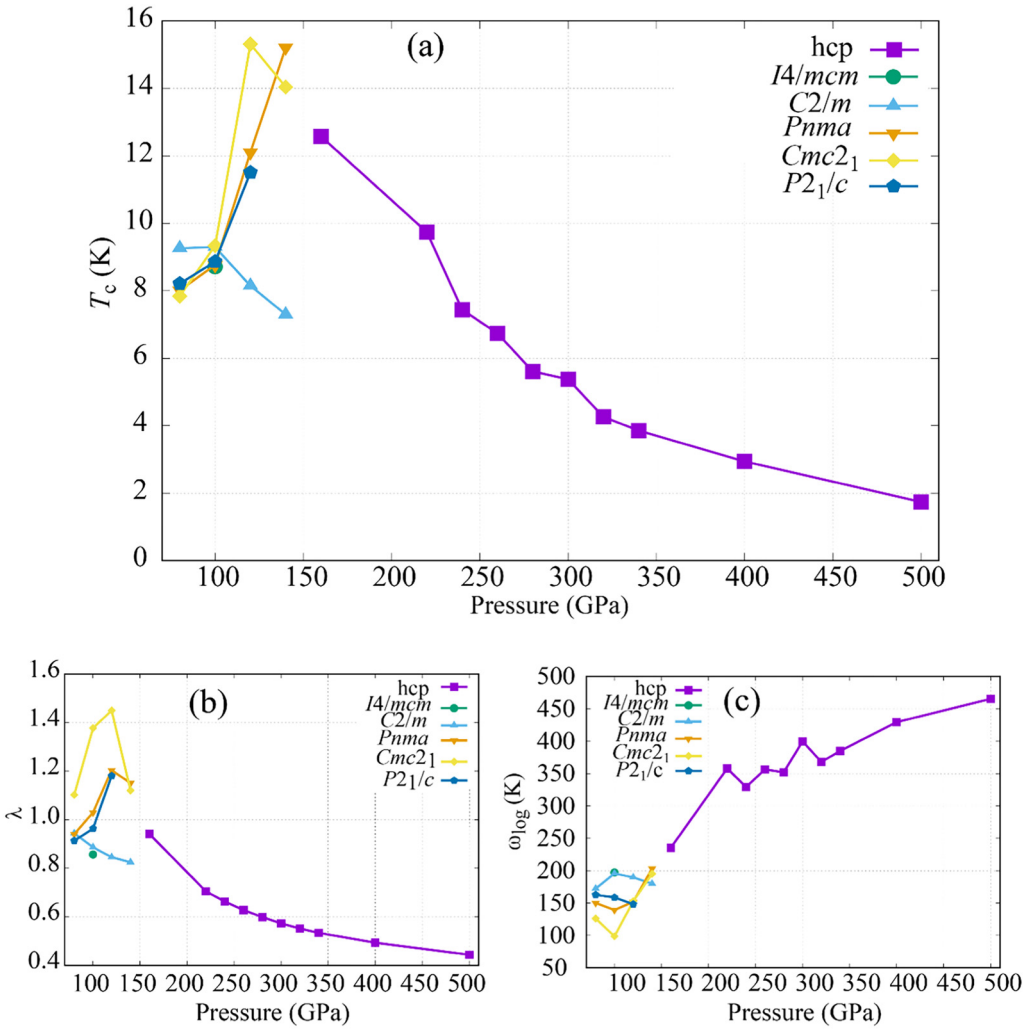

FIG. 3. (a) The pressure dependence of the superconducting transition temperature, T_c, of the hcp, *I*4/*mcm*, *C*2/*m*, *Pnma*, *Cmc*2$_1$, and *P*2$_1$/*c* structures. (b) The pressure dependency of the electron–phonon coupling constant. (c) The pressure dependence of the logarithmic average of the phonon frequency. The empirical parameter that describes the Coulomb screening, μ^*, is set to 0.13. The solid lines are guides to the eye.

100 and 120 GPa and that of the *I*4/*mcm* structure at 100 GPa are listed in Tables I–III in the supplementary material, respectively. The difference in atomic positions in the *C*2/*m* structure above and below 100 GPa is the 4*e* (1/4,1/4,0) or 4*f* (1/4,1/4,1/2) sites.

From 60 to 120 GPa, the *Pnma*, *Cmc*2$_1$, and *P*2$_1$/c structures are obtained as another group of the second-lowest enthalpy structures being potential candidates for the Sr-VI phase. The crystal structures of *Pnma*, *Cmc*2$_1$, and *P*2$_1$/c prepared using VESTA[21] are shown in Figs. 2(d)–2(f). Within this group, the *Pnma* structure has the same space group as the Ba-VI phase.[11] In considering the experimental results of Ref. 13 and the similarity with Ba-VI, the *Pnma* structure may be the most promising candidate for the Sr-VI phase. The *Pnma* and *Cmc*2$_1$, and *P*2$_1$/*c* structures are similar to each other. In fact, only when the tolerance value of the atomic positions of FINDSYM[22,23] identifying a space group is increased from 0.01 to 0.1, *Cmc*2$_1$ is distinguished from *Pnma*. With respect to enthalpy, these three structures are considered to be the same. In the powder diffraction patterns calculated using VESTA,[21] the patterns of these structures are very similar to each other as shown in Figs. S2(a)–S2(c) in the supplementary material.[11] The lattice constants, atomic positions, and atomic volumes of the *Pnma*, *Cmc*2$_1$, and *P*2$_1$/*c* structures at 100 GPa are listed in Tables I–III, respectively. The atomic positions are almost the same as the Ba-VI phase.[11] At 100 GPa, the pattern of the *Cmc*2$_1$ structure perfectly matches that of the *Pnma* structure. The deviation of the *Cmc*2$_1$ or *P*2$_1$/*c* structure from the *Pnma* structure is also very small. Therefore, it may be reasonable to consider these as representing the *Pnma* structure at 100 GPa. However, it is noted that at other pressure values, the structures show different T_c values, which will be discussed below.

Figure 3 shows the calculated T_c in this work for the hcp, *I*4/*mcm*, *C*2/*m*, *Pnma*, *Cmc*2$_1$, and *P*2$_1$/*c* structures from 80 to 500 GPa. The experimental data of T_c of compressed Sr up to 60 GPa were published by Mizobata *et al.*,[24] and the computational results were reported by Kim *et al.*[8] There is no information on T_c of compressed Sr over 60 GPa. In the pressure region shown by Mizobata *et al.*, T_c increased up to about 8 K. In our work, T_c increases up to around 9.3 K in the *C*2/*m* structure at 100 GPa, and then decreases with pressure. This is similar to the trend observed in the Sr-V phase.[13] Hence, we conjecture *C*2/*m* to be the most plausible approximate structure for the Sr-V phase.

In the *Pnma* structure, T_c increases up to about 15.9 K as the pressure increases up to 140 GPa. In the *Cmc*2$_1$ structure, T_c increases up to about 15.3 K as the pressure increases up to 120 GPa, and then decreases with pressure. In the *P*2$_1$/c structures, T_c increases up to about 11.5 K as the pressure increases up to 120 GPa. These three plausible structures *Pnma*, *Cmc*2$_1$, and *P*2$_1$/c are aggregated into the hcp structure at approximately 160 GPa (or around 140 GPa). It is particularly important to note that the pressure dependence of T_c for *Pnma*, *Cmc*2$_1$, and *P*2$_1$/*c* is mostly consistent with that of the experimental results obtained for Sr-VI.[13] This is a promising evidence that the structure of Sr-VI is either *Pnma*, *Cmc*2$_1$, or *P*2$_1$/*c*. If it is the same as for Ba,[11] the *Pnma* structure can be considered the most plausible structure.

The pressure dependence of T_c for the three structures in Fig. 3 shows that at 100 GPa, T_c is nearly identical. At this point, the *Pnma* structure is the most plausible candidate since the XRD patterns shown in the supplemental material (Fig. S2 in the supplementary material) almost overlap. However, at 120 and 140 GPa, T_c behaves quite differently in these three structures. Considering the experimental results where T_c increases with pressure within the Sr-VI phase and reaches a maximum of 13 K at 165 GPa in the hcp Sr-VII phase,[13] the *Pnma* structure in our calculations shows a higher T_c of 15.9 K at a relatively lower pressure of 140 GPa, while the *Cmc*2$_1$ structure reaches a maximum at 120 GPa and shows a sharp drop at 140 GPa. On the other hand, the *P*2$_1$/*c* structure shows an increase in T_c up to 120 GPa (11.5 K) and then becomes the hcp structure at 140 GPa. A careful comparison of the pressure dependence of T_c based on our calculations with detailed experimental results is needed to ascertain the actual structure in the Sr-VI phase.

At approximately 160 GPa, the lowest enthalpy structure becomes the hcp structure and represents the Sr-VII phase. This is consistent with the experimental results of Ito *et al.*[13] The enthalpies of the *Cc*, *I*4/*mcm*, and *C*2/*m* structures have higher enthalpy above around 160 GPa, and it is reasonable not to consider these as potential structures with further compression. Based on our structure search, there are three structures that should be compared, the hcp, dhcp, and fcc structures above 160 GPa pressurizing up to 2400 GPa as shown in Fig. 4. The plotted results were obtained through a structure search covering the tetragonal, trigonal, hexagonal, and cubic structures with cells containing four atoms. Moreover, to further validate the results, the structure search was performed at 600, 1200, 1600, 2000, and 2400 GPa using cells containing 16 atoms, which rendered results consistent with those obtained through smaller cells. The sequence of the phase transitions with increasing pressure is hcp (≈160 GPa) → dhcp (≈1000 GPa) → fcc (≈2200 GPa). The structural transitions from hcp to dhcp and then from dhcp to fcc indicate that as the pressure increases, the stacking of the close-packed structure from ABAB to ABAC and from ABAC to ABCABC results in lower enthalpy.

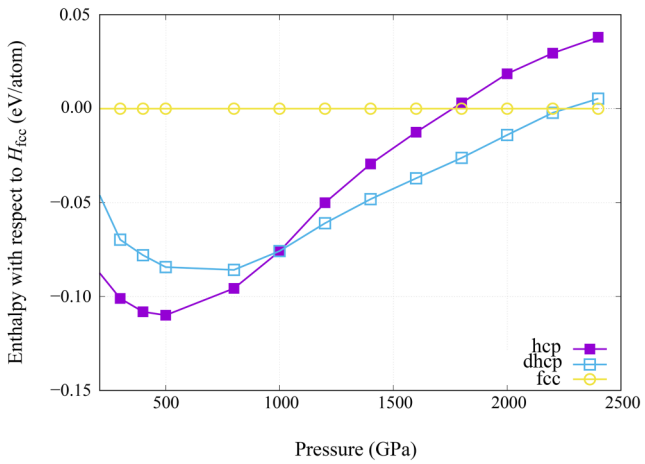

FIG. 4. The calculated enthalpy *H* of compressed Sr with respect to the enthalpy of the fcc structure as a function of pressure from 200 to 2400 GPa. The solid lines are guides to the eye.

The structural stability of these structures is confirmed through phonon calculations within a harmonic approximation, and the results are shown in Fig. 5. In the restricted calculations using small cells, structures with low enthalpy may not necessarily be dynamically stable; however, within the harmonic approximation, these structures are dynamically stable up to 2400 GPa.

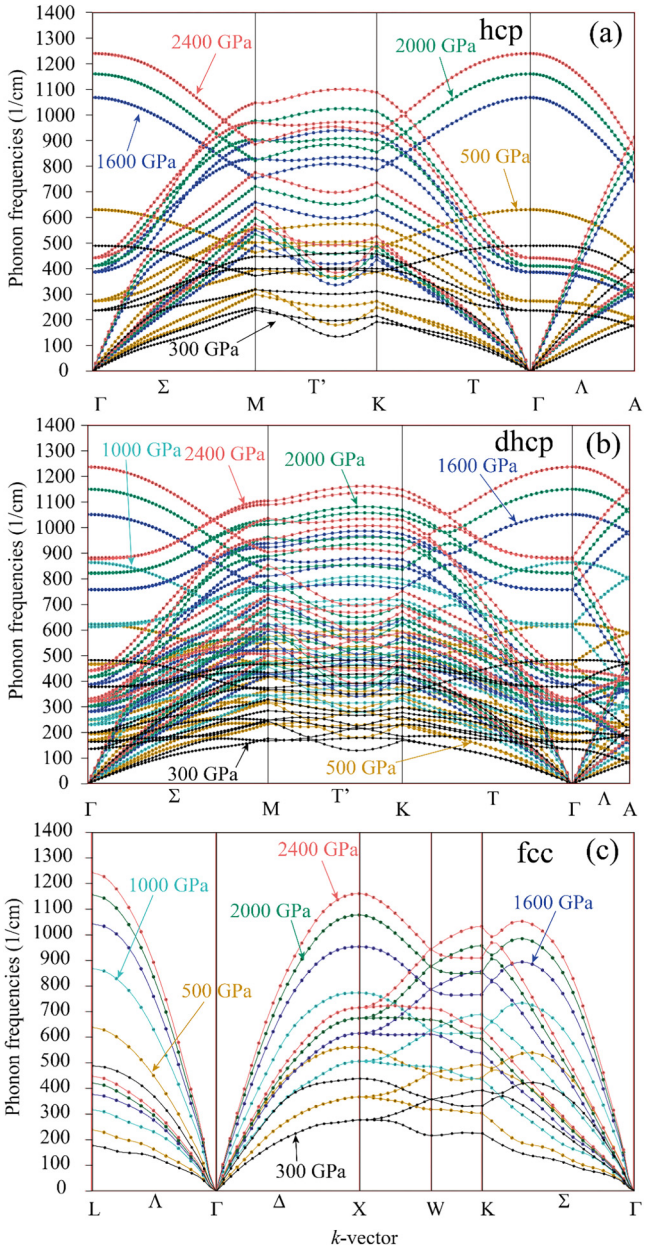

FIG. 5. The phonon dispersion curves of (a) the hcp, (b) dhcp and (c) fcc structures from 300 to 2400 GPa. The solid lines are guides to the eye.

After the transition to the hcp structure around 160 GPa, T_c decreases with pressure. Although not plotted in Fig. 3, as long as the hcp structure stays intact, the superconducting state survives beyond 1000 GPa with a decreasing T_c. At 1000 GPa, T_c is 0.65 K ($\lambda = 0.371$, $\omega_{log} = 664.4$ K). In Fig. 4, the hcp structure transforms to the dhcp structure at approximately 1000 GPa. In the dhcp structure, the superconducting state is stable and T_c at 1000 GPa is 1.1 K ($a = 2.1667$ Å, $c = 7.0549$ Å, $\lambda = 0.397$, $\omega_{log} = 639.6$ K) and T_c at 2000 GPa is 0.04 K. ($a = 2.0041$ Å, $c = 6.5234$ Å, $\lambda = 0.292$, $\omega_{log} = 811.7$ K). The dhcp structure transforms to the fcc structure at approximately 2200 GPa. The superconducting state of the fcc structure diminishes at around 2400 GPa, and T_c at 2400 GPa is 0.001 K ($a = 2.77$ Å, $\lambda = 0.246$, $\omega_{log} = 882.3$ K), and the value of λ is much smaller.

IV. CONCLUSIONS

We performed a structure search for highly compressed Sr using the first-principles calculations and determined the structures from 40 to 2400 GPa. In particular, the plausible candidate structures for the Sr-V and Sr-VI (low-temperature) phases from about 60–160 GPa and for the Sr-VII phase above 160 GPa were determined. The lowest and second lowest enthalpy groups in the pressure range of 60–160 GPa are considered to be the plausible structures corresponding to the Sr-V and Sr-VI phases, respectively. For these structures, the pressure dependence of T_c was calculated, and the results are consistent with the recent experimental results.[13] Based on our calculated structures and the conformity of T_c with the experimental results, $C2/m$ is the most plausible approximate structure for the Sr-V phase and $Pnma$, $Cmc2_1$, and $P2_1/c$ are the most plausible candidates for the low-temperature Sr-VI phase. The $Pnma$ structure shares the same space group structure with the Ba-VI phase. More detailed experimental investigations are required together with our results to ascertain the actual structure in the Sr-VI phase. Approximately above 160 GPa, the hcp structure is the most plausible candidate for the Sr-VII phase according to our calculations, and this is consistent with the recent experimental results. The hcp structure is dynamically stable up to around 1000 GPa and transforms to the dhcp structure, and the dhcp structure then transforms to the fcc structure at around 2200 GPa. The superconducting state remained intact through these structural phase transitions, although with a decreasing T_c with increasing pressure.

SUPPLEMENTARY MATERIAL

See the supplementary material for information on the 100 GPa structures in the text and the XRD patterns calculated with VESTA using them.

ACKNOWLEDGMENTS

This work was supported by JSPS KAKENHI, a Grants-in-Aid for Scientific Research (C) (Nos. 19K037170, 23K04518a, and 24K069590).

AUTHOR DECLARATIONS

Conflict of Interest

The authors have no conflicts to disclose.

Author Contributions

Masaaki Geshi: Conceptualization (lead); Data curation (lead); Formal analysis (lead); Funding acquisition (lead); Investigation (lead); Methodology (lead); Project administration (lead); Resources (lead); Software (lead); Supervision (lead); Validation (lead); Visualization (lead); Writing – original draft (lead); Writing – review & editing (lead). **Hiroki Funashima:** Methodology (supporting); Software (equal); Writing – original draft (supporting); Writing – review & editing (supporting). **Gayan Prasad Hettiarachchi:** Formal analysis (supporting); Investigation (supporting); Writing – original draft (equal); Writing – review & editing (equal).

DATA AVAILABILITY

The data that support the findings of this study are available from the corresponding author upon reasonable request.

REFERENCES

[1]D. B. McWhan and A. Jayaraman, "Crystal structure of strontium metal above 35 kbar and its relation to ytterbium," Appl. Phys. Lett. **3**, 129 (1963).
[2]H. Olijnyk and W. B. Holzapfel, "Phase transitions in alkaline earth metals under pressure," Phys. Lett. A **100**, 191 (1984).
[3]D. R. Allan, R. J. Nelmes, M. I. McMahon, S. A. Belmonte, and T. Bovornratanaraks, "Structures and transitions in strontium," Rev. High Pressure Sci. Technol. **7**, 236 (1998).
[4]T. Bovornratanaraks, D. R. Allan, S. A. Belmonte, M. I. McMahon, and R. J. Nelmes, "Complex monoclinic superstructure in Sr-IV," Phys. Rev. B **73**, 144112 (2006).
[5]M. I. McMahon, T. Bovornratanaraks, D. R. Allan, S. A. Belmonte, and R. J. Nelmes, "Observation of the incommensurate barium-IV structure in strontium phase V," Phys. Rev. B **61**, 3135 (2000).
[6]A. Phusittrakool, T. Bovornratanaraks, R. Ahuja, and U. Pinsook, "High pressure structural phase transitions in Sr from *ab initio* calculations," Phys. Rev. B **77**, 174118 (2008).
[7]P. Srepusharawoot, W. Luo, T. Bovornratanaraks, R. Ahuja, and U. Pinsook, "Evidence of a medium-range ordered phase and mechanical instabilities in strontium under high pressure," Solid State Commun. **152**, 1172 (2012).
[8]D. Y. Kim, P. Srepusharawoot, C. J. Pickard, R. J. Needs, T. Bovornratanaraks, R. Ahuja, and U. Pinsook, "Phase stability and superconductivity of strontium under pressure," Appl. Phys. Lett. **101**, 052604 (2012).
[9]P. Tsuppayakorn-aek, W. Chaimayo, Y. Pinsook, and T. Bovornratanaraks, "Existence of the β-tin structure in Sr: First evidence from computational approach," AIP Adv. **5**, 097202 (2015).
[10]H. Katzke and P. Tolédano, "Competition between Burgers mechanism and bain deformation in alkaline-earth metals: Host-guest structures of barium and strontium," Phys. Rev. B **75**, 174103 (2007).
[11]S. Desgreniers, J. S. Tse, T. Matsuoka, Y. Ohishi, Q. Li, and Y. Ma, "High pressure–low temperature phase diagram of barium: Simplicity versus complexity," Appl. Phys. Lett. **107**, 221908 (2015).
[12]D. E. Jackson, D. VanGennep, Y. K. Vohra, S. T. Weir, and J. J. Hamlin, "Superconductivity of barium-VI synthesized via compression at low temperatures," Phys. Rev. B **96**, 184514 (2017).
[13]T. Ito, Y. Kara, Y. Nakamoto, M. Sakata, K. Shimizu, H. Fujihisa, S. Kawaguchi, N. Hirao, and Y. Ohishi, Superconductitivy and crystal structure of strontium in alkaline earth metal under high pressure, in *Meeting Abstracts of 2020 Annual Meeting of the Physical Society of Japan*, *75.1 (18pPSA-11)* (The Physical Society of Japan, 2020), in Japanese.
[14]M. Geshi and H. Funashima, "First-principles study for high-pressure tellurium near a transition from bcc to fcc," J. Phys. Soc. Jpn. **89**, 124603 (2020).
[15]P. Giannozzi, O. Andreussi, T. Brumme, O. Bunau, M. Buongiorno Nardelli, M. Calandra, R. Car, C. Cavazzoni, D. Ceresoli, M. Cococcioni, N. Colonna, I. Carnimeo, A. Dal Corso, S. de Gironcoli, P. Delugas, R. A. DiStasio, A. Ferretti, A. Floris, G. Fratesi, G. Fugallo, R. Gebauer, U. Gerstmann, F. Giustino, T. Gorni, J. Jia, M. Kawamura, H.-Y. Ko, A. Kokalj, E. Küçükbenli, M. Lazzeri, M. Marsili, N. Marzari, F. Mauri, N. L. Nguyen, H.-V. Nguyen, A. Otero-de-la-Roza, L. Paulatto, S. Poncé, D. Rocca, R. Sabatini, B. Santra, M. Schlipf, A. P. Seitsonen, A. Smogunov, I. Timrov, T. Thonhauser, P. Umari, N. Vast, X. Wu, and S. Baroni, "Advanced capabilities for materials modelling with QUANTUM ESPRESSO," J. Phys.: Condens. Matter **29**, 465901 (2017).
[16]J. P. Perdew, K. Burke, and M. Ernzerhof, "Generalized gradient approximation made simple," Phys. Rev. Lett. **77**, 3865 (1996).
[17]We used the pseudopotential, Sr.pbe-spn-rrkjus_psl.1.0.0.UPF, see http://www.quantum-espresso.org.
[18]M. Geshi, H. Funashima, and G. P. Hettiarachchi, "Study of compressed sulfur based on reliable first-principles calculations," Phys. Rev. B **104**, 104106 (2021).
[19]P. B. Allen and R. C. Dynes, "Transition temperature of strong-coupled superconductors reanalyzed," Phys. Rev. B **12**, 905 (1975).
[20]J. Whaley-Baldwin, M. Hutcheon, and C. J. Pickard, "Superconducting incommensurate host-guest phases in compressed elemental sulfur," Phys. Rev. B **103**, 214111 (2021).
[21]K. Momma and F. Izumi, "*VESTA 3* for three-dimensional visualization of crystal, volumetric and morphology data," J. Appl. Crystallogr. **44**, 1272 (2011).
[22]H. T. Stokes, D. M. Hatch, and B. J. Campbell, *FINDSYM* (ISOTROPY Software Suite, iso.byu.edu, 2024).
[23]H. T. Stokes and D. M. Hatch, "Program for identifying the space group symmetry of a crystal," J. Appl. Crystallogr. **38**, 237 (2005).
[24]S. Mizobata, T. Matsuoka, and K. Shimizu, "Pressure dependence of the superconductibity in strontium," J. Phys. Soc. Jpn. **76**(Suppl. A), 23 (2007).

Search for Promising Structures and Superconductivity in High-Pressure Sr through First-Principles Calculations

Masaaki Geshi[1], Hiroki Funashima[2], Gayan Prasad Hettiarachchi[1]

[1] *R^3Institute for Newly-Emerging Science Design, Osaka University, 1-2 Machikaneyama, Toyonaka, Osaka 560-0043, Japan*

[2]*Department of Comprehensive Engineering, Kindai University Technical College, 7-1 Kasugaoka, Nabari, Mie 518-0459, Japan*

I. LATTICE PARAMETERS AND ATOMIC POSITIONS

As typical structural information, the lattice parameters and the atomic positions at 100 GPa are summarized in TABLES SI-SIV for the $C2/m$, $I4/mcm$, and Cc structures. The atomic positions of the $C2/m$ structure take the same Wyckoff position at 80 GPa and 100 GPa and the same Wyckoff position at 120 GPa and 140 GPa. The difference is the 4*f* and 4*e* sites.

TABLE SI

The atomic positions of the $C2/m$ structure at 100 GPa. The lattice parameters are *a*=10.9800, *b*=9.2578, *c*=4.9866 Å, and β=111.4983 deg.

	Wyckoff letter	x	y	z	Wyckoff position
Sr1	*4f*	0.25000	0.25000	0.50000	(1/4, 1/4, 1/2)
Sr2	*4i*	0.61738	0.00000	0.69906	(x, 0, z)
Sr3	*4g*	0.00000	0.64869	0.00000	(0, y, 0)
Sr4	*8j*	0.33359	0.35196	0.00831	(x, y, z)
Sr5	*4i*	0.71425	0.00000	0.29011	(x, 0, z)
Sr6	*4h*	0.00000	0.74980	0.50000	(0, y, 1/2)
Sr7	*4i*	-0.05242	0.00000	0.70186	(x, 0, z)

TABLE SII

The atomic positions of the $C2/m$ structure at 120 GPa. The lattice parameters are *a*=10.6999, *b*=9.0875, *c*=4.8930 Å, and β=111.2771 deg.

	Wyckoff letter	x	y	z	Wyckoff position
Sr1	4*g*	0.00000	0.25066	0.00000	(0, y, 0)
Sr2	*4i*	0.28619	0.00000	0.20983	(x, 0, z)
Sr3	*8j*	0.16611	0.14807	0.49117	(x, y, z)
Sr4	*4h*	0.00000	0.35086	0.50000	(0, y, 1/2)
Sr5	*4i*	0.38208	0.00000	0.80073	(x, 0, z)
Sr6	*4e*	0.25000	0.25000	0.00000	(1/4, 1/4, 0)
Sr7	*4i*	-0.05282	0.00000	0.20046	(x, 0, z)

TABLE SIII

The atomic positions of the $I4/mcm$ structure at 100 GPa. The lattice parameters are *a*=6.5486 and *c*=11.0003 Å.

	Wyckoff letter	x	y	z	Wyckoff position
Sr1	4*c*	0.00000	0.00000	0.00000	(0, 0, 0)
Sr2	8*h*	0.14539	0.64539	0.00000	(x, x+1/2, 0)
Sr3	16*l*	0.64932	0.14932	0.16635	(x, x+1/2, z)
Sr4	4*a*	0.00000	0.00000	0.25000	(0, 0, 1/4)

TABLE SIV

The atomic positions of the Cc structure at 100 GPa. The lattice parameters are a=7.4761, b=6.5499, c=9.8657 Å, and β=103.017 deg.

	Wyckoff letter	x	y	z	Wyckoff position
Sr1	4*a*	0.05400	0.10557	-0.04449	(x, y, z)
Sr2	4*a*	0.41830	0.09808	0.02450	(x, y, z)
Sr3	4*a*	0.65568	0.24915	-0.09542	(x, y, z)
Sr4	4*a*	0.89638	0.40238	0.78917	(x, y, z)
Sr5	4*a*	0.26103	0.39238	0.85811	(x, y, z)
Sr6	4*a*	0.08842	0.09969	0.68905	(x, y, z)
Sr7	4*a*	0.72310	0.10152	0.62501	(x, y, z)
Sr78	4*a*	0.40308	0.25213	0.65411	(x, y, z)

II. POWDER DIFFRACTION PATTERNS

The powder diffraction patterns obtained using VESTA are shown in FIG. S1 for the $C2/m$, $I4/mcm$, and *Cc* structures and FIG. S2 for the $Pnma$, $Cmc2_1$, and $P2_1/c$ structures at 100 GPa.

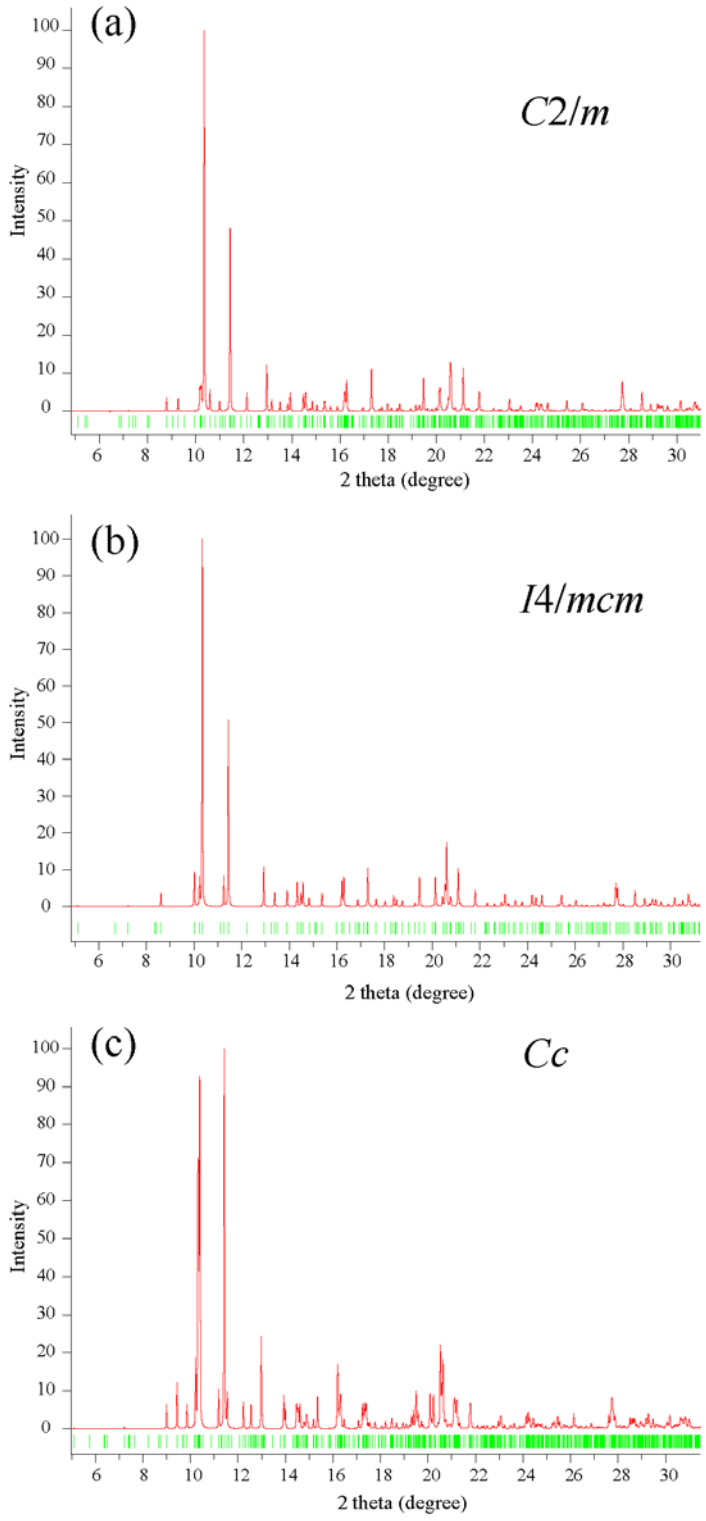

FIG. S1 (Color online)

The powder diffraction patterns of the $I4/mcm$, $C2/m$, and Cc structures calculated using VESTA [1]. The wavelength λ is 0.4128 Å [2].

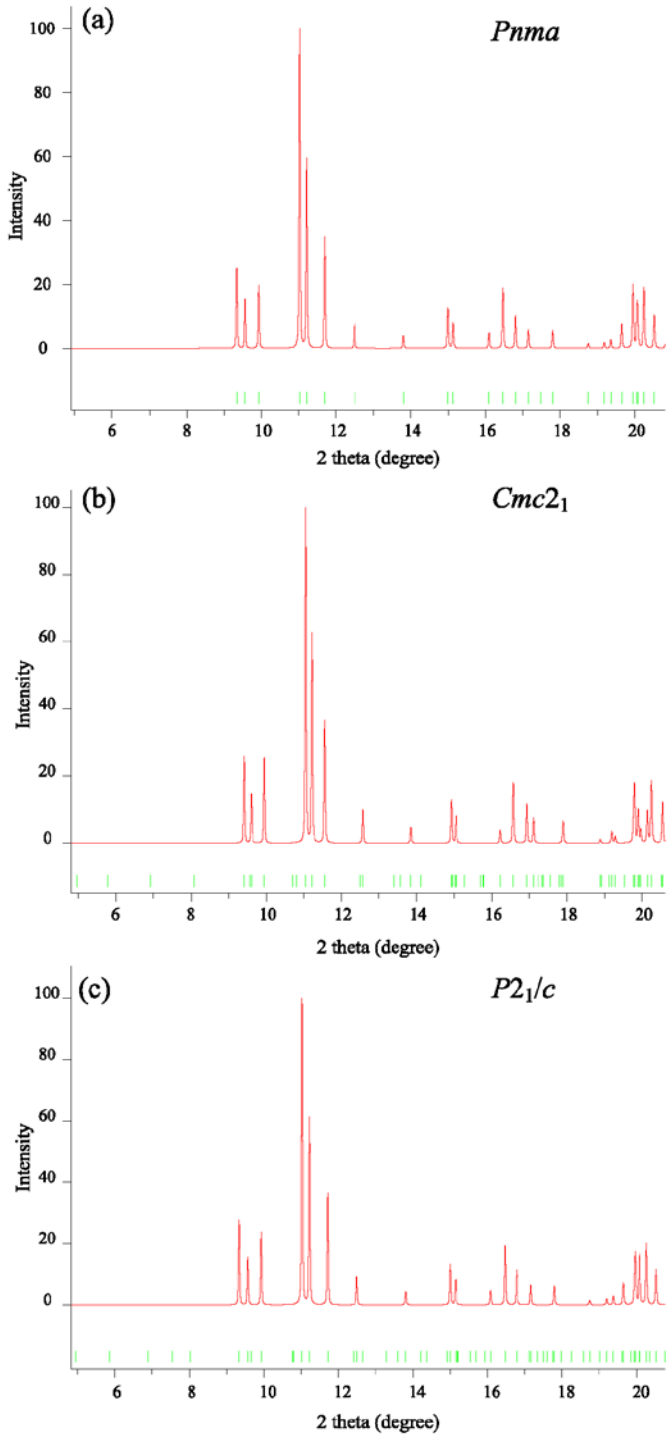

FIG. S2 (Color online)

The powder diffraction patterns of the $Pnma$ and $Cmc2_1$, $P2_1/c$ structures calculated using VESTA [1]. The wavelength λ is 0.4128 Å [2].

References:

1. https://jp-minerals.org/vesta/en/
2. Y. Nakamoto, M. Sakata, K. Shimizu, and N. Hirao, Crystal Structure and Superconductivity in Alkaline Earth Metal, Strontium, under High Pressure and Low Temperature, SPring-8/SACLA Research Achievements **9**, 5(2021). (DOI 10.18957/rr.9.1.5)